Engineering Science & Technology
http://ojs.wiserpub.com/index.php/EST/

UNIVERSAL WISER PUBLISHER

Research Article

# Adaptive Spectrum Sensing in Cognitive Radio Employing Multitaper Method and Higher-Order STBC Techniques

**Ahmed O. Abdul Salam[1*], Ray E. Sheriff[2], Saleh R. Al-Araji[3], Kahtan Mezher[3], Qassim Nasir[4]**

[1]Formerly with Faculty of Engineering and Informatics, University of Bradford, Bradford, UK
[2]Department of Computer Science, Edge Hill University, Lancashire, UK
[3]Formerly with College of Engineering, Khalifa University, Abu Dhabi, UAE
[4]College of Engineering, University of Sharjah, Sharjah, UAE
E-mail: aoa_salam@yahoo.com

**Received:** 30 April 2024; **Revised:** 2 September 2024; **Accepted:** 9 October 2024

**Abstract:** The effects of the non-parametric multitaper method (MTM) and symmetrical higher-order space-time block-code (STBC) with full diversity techniques on the performance of spectrum sensing (SS) in cognitive radio (CR) systems are studied. The overall wireless link performance can be improved by using the STBC techniques to combat the multipath fading effects in wireless channels. The MTM is integrated with the STBC for spectrum estimation (SE), which will be termed multitaper spectrum estimation (MTSE)-STBC, and the given analysis of which is developed using the quadrature form approximation. Also, classical SE algorithms commonly focus on a fixed performance assessment method based on predefined false alarms or detection probabilities. Licensed users need to be protected against interference that opportunistic users might cause. An appropriate thresholding policy that varies concerning the designated values of false alarm and detection rates can achieve such protection. Utilization factors are instrumental in providing further protection for licensed users or occupied spectrum holes, and they need to be determined in advance and adopted in the detection policy. If utilization factors are not desirable, then a fine selection of appropriate threshold values will need to be decided as they have a major impact on the overall error probability performance. Using analytical and simulation methods, the assessment results revealed improved performance of the MTSE-STBC compared to other classical methods such as the Periodogram especially in the aspects of efficient transmission and less error probability. The proposed adaptive thresholding technique also proved useful in coping with different SE settings.

***Keywords*:** spectrum sensing, cognitive radio, multitaper, STBC, threshold adaptation, utilization factor

## 1. Introduction

The shear drive for the radio frequency spectrum to be efficiently utilized has become overwhelming in ubiquitous wireless communication systems. This is mainly due to the perpetual advent of unprecedented social and commercial services supplied remotely through high data rate channels. The cognitive radio (CR) system based on the software-defined radio (SDR) concept has been recently recognized as a game-changing technology. It has emerged as a competent candidate with significant potential to address most of the existing pressing demands [1]-[7]. Smart wireless appliances that embark on evolving CR systems enjoy multiple adaptation properties to achieve better network and application performance. They can accordingly detect the environment and dynamically adapt their internal parameters,


DOI: https://doi.org/10.37256/est.6120254856

such as transmission waveforms, network protocols, spectrum utilization, and channel access methods.

A perception of the current and future trends of advancement and development of newly emerging smart applications indicates a paradigm shift towards the involvement of CR systems. Smart grid, public safety, machine-to-machine (M2M), mobile cloud computing, and wireless medical are just a few applications of networks and communications, among many others [3], [4]. While in the confined context of cellular networks, there is no dispute that the 5G is picking up at a pace that is leaving even some industry veterans breathless. Owing to the attractive capabilities that CR systems can offer, they are thus expected to vigorously participate in achieving the potential demands of massive users under such 5G parasol. This can be embraced by invoking the six challenges that have not been effectively addressed by the current 4G platform, namely, higher capacity, higher data rate, lower end-to-end latency, vast connections, less cost, and perceived high quality of service (QoS) [5], [6]. Therefore, serious investments to innovate new wireless communication technologies that are more cognitive, efficient, and realizable have become more pressing than before.

The following help abreast the foundation technologies and works related to the challenges addressed in this article.

## 1.1 *Sensing foundation*

It is widely recognized that the issue of spectrum estimation (SE), or equivalently spectrum sensing (SS), is a challenge, especially in broadband applications. Unlicensed secondary users (SUs) naturally endeavor to constantly monitor the activities of licensed primary users (PUs) in noisy environments. SUs hence try to coexist alongside PUs without making any harmful interference. Spectrum bands rarely used by PUs are commonly known as "white spaces (WSs) or holes" and are readily available for opportunistic access by SUs [1]-[8]. The existence of such WSs is mostly governed by PUs' dynamic activities that follow a random pattern within a particular CR network (CRN) [2], [4], [9]. SUs are to perform SE either sequentially or sporadically to detect the recurrence of PUs so that they can stop or limit their destructive interaction. Also, the SE can be accomplished either temporally or spatially [8]. In temporal SE, WSs are created by PUs not occupying the spectrum bands of interest during the sensing time; hence, these spectrum bands can be utilized by SUs in the current time slot. In spatial SE, spectrum bands are occupied by PUs in restricted geographical areas, and as such the same bands can be considered as WSs outside the restricted areas and hence can be exploited by SUs located fairly outside those areas.

## 1.2 *FCC & TVWS regulations*

WSs are distinct among black and grey spaces that are severely and moderately used by PUs, respectively. In an effort for legalization, significant academic and industrial collaborations have contributed to the successful publicity of the IEEE 802.22 standard by the Federal Communication Commission (FCC) in 2008. This standard defines a scheme on wireless regional area networks (WRANs), which supports last-mile broadband wireless access over unused TV white spaces (TVWSs) for large rural areas [2]-[4], [7], [8], [10]-[14]. The FCC eventually paved the way to use spectrum frequencies in the industrial, scientific, and medical (ISM) for commercial opportunistic transmissions. After all, the TVWSs constitute only a small portion of the ISM bands. Among several practical testbeds, the experiment of quantifying the TVWSs for spectrum opportunistic reuse and SUs deployment in Malaysia can be cited [15].

## 1.3 *PHY & MAC layers*

All the known SS techniques typically occur at the physical layer (PHY) [2], [4], [8], [11], [13], which is also the aim of this work. This is where the digital front end of SDR hardware resides and is particularly meant for signal processing functionalities. While, on the other hand, the spatiotemporal coexistence of multiple PUs and SUs, without causing any harmful interference, can be accomplished at the medium access layer (MAC) using the dynamic spectrum access (DSA) software management protocols [1]-[4], [11], [13].

## 1.4 *Sensing surveys*

Surveys on the evolutio n and versatility of SE in wireless CR systems are numerous and a notable few are selected here among many others in the open literature [4], [8], [10]-[15]. Without loss of generality, the SE framework can be either cooperative or non-cooperative. In the first framework, CR terminals relay their SE results to a centralized fusion system, and the center then informs all terminals and orchestrates their access accordingly. In the second framework, however, each CR terminal acts individually without sharing the SE outcome with any other node or terminal. Both frameworks broadly involve reactive or proactive SE modes of operation, depending on how CR systems search for WSs [4], [10], [13]. A CR in the reactive mode operates on an on-demand basis and starts SS only when it has some data to transmit. A CR in the proactive mode aims at minimizing the delay incurred in finding an idle band by maintaining a list of one or more licensed bands currently available through periodic SS. The enhanced data broadcast responsiveness in proactive SE comes at the expense of higher computation overhead and longer latency. A trade-off between rate and reliability must be eventually optimized.

The SE techniques under the above-indicated two frameworks can be generally classified into three main categories. The first category is the guided SE where the signal and noise attributes are well-informed, and under which the cyclostationary detection (CSD), the matched filter (MF), and the likelihood ratio test (LRT) techniques can be identified [2], [4], [8], [10]-[14]. The second category is the semi-guided or semi-blind SE, where only the noise attribute is informed, and as such wavelet-based sensing and energy detection (ED) can be placed under this category [2], [4], [7], [8], [10]-[15]. While the third category is unguided or blind SE, where no prior information is provided, and under which the blindly combined ED detections, the covariance (COV), and the emerging maximum to minimum eigenvalue (MME) can be recognized [2], [4], [8], [13], [14].

Other non-statistical SS techniques can also be found in the literature. For example, a boosted tree algorithm (BTA) to mitigate SS data falsification (SSDF) by obtaining reliable identification of PU's channel in the framework of the cooperative SS scenario was proposed in [16]. A recent discussion around compressive SS methods appropriate for 5G communication systems can be found in the mini-review by [17]. A scheme of SS based on a Convolutional Autoencoder (CAE) for application in CRNs and by modeling the channel occupancy as an anomaly detection problem was addressed in [18]. On the few aspects of cooperative spectrum sharing a structure of multi-agent systems and game theory, and a blockchain of smart contracts for sustainable CRNs and beyond 5G wireless communication can be found in [19], [20], respectively, among many other studies.

## 1.5 *Multitaper method*

Arriving at an optimal SE policy that meets the coverage and transmission performance settings of various CRNs is a crucial issue, as evident from the previous sections. Along this perspective, the non-parametric multitaper method (MTM) was favorably voiced as an attractive opinion as an alternative SE scheme [8], [12], [21]-[25]. The ingredient of discrete prolate spheroidal (DPSS) wave function as prototype filter coefficients makes the MTM more appealing. These functions, also known as the Slepian sequence, were characterized by two important properties: 1) the main lobe has the maximum energy concentration, and 2) orthonormal [12]. Balanced trade-offs in the bias-variance dilemma can be achieved by employing orthogonal data sets to enhance the spectral estimate resolution. The robust leakage control in the out-of-bound (OOB) spectrum manifested by the tapering process renders the performance of SE based on MTM (MTSE) outstanding compared with other techniques that belong to the same family.

## 1.6 *MIMO techniques*

The techniques of multiple-input multiple-output (MIMO) techniques are envisaged to continue in the present and future wireless communication systems due to their specular versatilities. The MIMO regimes are considered an unavoidable option to combat the harmful effects of fading channels. They are competent to achieve higher speeds with less error rates and significantly enhance systems capacity and reliability [26]. The literature on MIMO-based SE techniques is diverse. For instance, multi-antenna-based SS methods and the generalized LRT ratio test (GLRT) paradigm were reported in [27], [28]. The proposed methods, like ED, estimator-correlator (EC), and arithmetic to geometric mean (AGM), utilize the eigenvalues of the sample covariance matrix of the received signal vector through

single-input multiple-output (SIMO) scheme. The GLRT test approach using the MIMO arrangement and interrogating the eigenvalues of the sample covariance matrix was given in [28], [29]. In a recent SE work, invariant constant false-alarm rate eigenvalue-based (EVB) detectors for MIMO, using the higher order moments of the sample covariance matrix eigenvalues, conducted in the framework of separating function estimation test (SFET) was proposed in [30]. These sample studies, and several others, undeniably accorded to the SS performance improvement realized by exploiting the varieties of multi-antenna options.

## 1.7 *STBC techniques*

System gains and diversity can be further improved by employing space-time coding techniques such as the space-time block code (STBC) and the space-time trellis code (STTC). Owing to their simple design and low complexity receivers, orthogonal STBCs compared to STTCs are more attractive to the coding community. A linear decoding scheme such as the maximal likelihood (ML) can be easily implemented on the STBC receiver [26], [31]. Most applications that adopt MIMO systems in their standards use STBC as an option. It is hence compelling to consider SS implementation for STBCs to reduce their complexity. The basic STBC form was developed by Alamouti and from which other STBCs can be derived. This paper will consider a few examples of symmetrical higher-order STBCs that can achieve full diversity order irrespective of coding gain, which is normally of trivial implication to SE applications.

## 1.8 *Threshold adaptation*

The issue of threshold adaptation in SE for CR systems is considered a challenging task. The threshold function is a typical convex optimization problem and is expressed in two explicit variables the missed detection and false alarm probabilities [32]-[34]. The SE performance is highly governed by these probabilities, which are threshold value dependent. A perfect knowledge of the noise power is essential to administer the SE decision threshold. The failure to know the noise will not result in the desired false alarm probability and eventually renders the SE performance susceptible to errors. The multiple tasks of minimizing SE error, achieving better PUs protection, and improving the spectrum utilization efficiency can all be achieved by a decision threshold that is suitably selected. The higher the threshold value, the better detection probability and protection against indivertible interference to PUs is achieved. The lower the threshold value, the higher the false alarm probability, and less PUs protection is generated. Therefore, an adequate threshold adaptation policy is mandatory for trade-offs between the two situations. As will be shortly seen in the context, thresholds heavily rely on the statistical features of transmission signaling in CR systems. Worth noting is that prevailing adaptive threshold studies in the literature were mainly addressed in the context of ED configuration only (or equivalently the PSE in the analysis of this paper), and the impact of STBC (or MIMO) configuration attempted here is in the same direction of previous efforts in [24], [25].

## 1.9 *Motivation*

As highlighted above, and to the authors' best knowledge, the adoption of STBC schemes for SE has been seldom attempted [35]-[37]. For instance, the STBC featuring a multiple-input single-output (MISO) scheme in the process of spectrum reporting within each cluster of a fusion decision center aiming at sharing with multiple cooperative CR terminals was suggested [35], [36]. An ED involving the combination of a MIMO-STBC scheme and an eigen-based detector (EBD) to examine the observation COV matrix for a single CR node was addressed [37]. A higher-order moments-based STBC scheme using ED for SE was proposed in [38]. However, the earlier studies did not elaborate on the MTSE-STBC in a broader scope or address the deployment of higher-order STBC schemes in SS applications for CR systems. A recent article referencing the adaptive thresholding of the MTSE paradigm for SS in CR systems can be identified [23]. The adaptation was performed by estimating the noise and the signal powers to adjust the noise fluctuation and achieve an efficient trade-off between detection and false alarm probabilities. The study of [23] was conducted using single-input single-output (SISO) antennas, and it shed a good synopsis of the MTSE supremacy compared to the ED performance for adaptive and non-adaptive SS applications in CR environments. Furthermore, two new studies that adopted the MTSE-STBC for SS can be reported [24], [25]. Both studies employed low-order STBC schemes, while the latter separately tackled the issue of threshold adaptation requirements. This paper endeavors

to extend the work by [24], [25] and elaborates more on the impact of employing higher-order STBC schemes and thresholding techniques.

### 1.10 *Contribution*

The need for reliable detection strategies of the poorly utilized spectrum is paramount to the design of CR systems. Capitalizing on the above given and recent developments in this regard, this paper endeavors to contribute towards achieving a consistent and seamless SE style without extra overhead burden. Inspired by the growing interest in the robust features of MTSE and multi-antenna orthogonal codes, they are thus merited in this work. The following specific contributions can be summarized:

1. Design an optimal local SS paradigm using MTSE-STBC based on the Neyman-Pearson (NP) hypothesis test framework as a special case of the LLT rule given the circumstances.

2. Develop a novel MTSE-STBC model using the quadratic form approximation, aiming at detection improvement and thereby enabling the low signal-to-noise (*SNR*) regime, with the necessary performance indicators.

3. Conduct a performance assessment comparison of the proposed MTSE-STBC concerning traditional SE techniques, like Periodogram, and examine the spectrum tapering requirements and detection accuracies.

4. Tackle high-order STBC schemes and examine their effects on the MTSE statistical performance metrics.

5. Put together the essential analysis required to achieve a particular threshold adaptation policy in the STBC configuration and quantify its potential aspect on the designated performance measures.

6. Assess the range of utilization factors to protect PUs or let SUs occupy spectrum holes effortlessly.

### 1.11 *Mathematical notations*

Boldface uppercase and lower letters denote matrices and vectors; non-boldface uppercase and lower letters denote scalars. The symbols $(.)^{\mathrm{T}}$, $(.)^{*}$, $(.)^{\dagger}$, and $\|.\|_{\mathrm{F}}$ represent transpose, complex conjugate, Hermitian, and Frobenius norm operators. $j=\sqrt{-1}$ stands for imaginary, $\mathrm{Tr}(.)$ is the trace, $\Re(.)$ and $\Im(.)$ are the real and imaginary factors, and vec(.) is the vector stacking. The $\forall$, or $\in$, is all elements in a space, and $\mathcal{CN}(.,.)$ refers to the circular Gaussian complex prcess.

## 2. CR for sensing scenario

The FCC catered for the SE intervals assignment at the start of each data frame of SUs in the IEEE 802.22 standard [39]. Consider a local SE scenario comprising several PUs of unknown statuses and SUs working in the same band of interest. A diagram showing the PUs' statuses and SUs' periodic sensing frame structures is given in Figure 1.

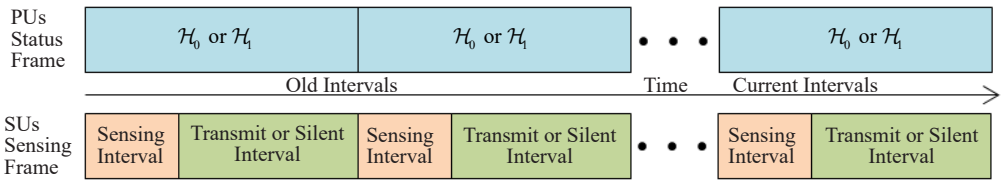


**Figure 1.** A pictorial of the unknown PUs activity and the SUs periodic sensing frames structure

The activity statuses of PUs are assumed unaltered during each complete frame of SUs. The sensing intervals in the front of SUs frames are aimed at monitoring the presence of PUs. The SUs are then to suitably decide whether to transmit data or keep silent in the remaining portion of each frame. The sensing time is usually optimized relative to the achievable throughput determined by each technology. Throughputs are normally governed by the sensing mode whether active (proactive) or quiet (silent or reactive) [4], [10], [13], threshold level, and the number of samples dedicated for sensing duration besides other requirements [40]. Sophisticated gears, such as MTM, can be used for the

fine SE, while the ED can be used for the coarse SE in each frame [39].

## 3. STBC signal modelling

Suppose a wireless channel of flat-fading or slow-fading Rayleigh effect. Assume the sensing time is very short compared with the channel coherence time and hence the channel gain can be considered time-invariant during the sensing process. Consider an $M$-ary signal constellation sequence of $K$ length is aimed at transmission through $N_t$ transmit and $N_r$ receive antennas and over $N_s$ time intervals. The normalized baseband signal at the $i^{th}$ receive antenna can be denoted as [27], [29]-[31], [37], [41], [42]:

$$y_i(k) = \sum_{j=1}^{N_t} h_{i,j} x_j(k) + w_i(k), \ \nabla i \in [1,\ N_r],\ k \in [1,\ K] \tag{1}$$

and defining the quasi-static $N_r \times N_t$ channel gain matrix:

$$\mathbf{H} = \begin{bmatrix} h_{1,1} & h_{1,2} & \cdots & h_{1,N_t} \\ h_{2,1} & h_{2,2} & \cdots & h_{2,N_t} \\ \vdots & \vdots & \ddots & \vdots \\ h_{N_r,1} & h_{i,j} & \cdots & h_{N_r,N_t} \end{bmatrix} \tag{2}$$

For ease, ignore the time index, the expression in (1) can hence take the linear matrix form below:

$$\mathbf{Y} = \mathbf{HX} + \mathbf{W} \tag{3}$$

where $\mathbf{X}$ is the $N_t \times 1$ complexed valued constellation transmitted over $N_s$ time intervals and stands for the STBC generator matrix in which the original information symbols reside. For presentation clarity and consistency, it is important to realize that the assumption of sending $M$ complex constellation over $N_s = M$ time intervals is adopted here to discuss symmetrical STBC schemes only. Other nonsymmetrical STBC forms are widely known in the literature, which constitute deviation between the STBC time intervals than $M$ constellation size and will not be continued further in this article. Another invariable assumption in the literature, which will also be followed in this work, is that the additive noise vector $\mathbf{W}$ of size $N_t \times 1$ is deliberated as independent and identically distributed (iid) zero-mean circularly symmetrical complex Gaussian (ZMCSCG) noise and denoted by $\mathcal{CN} \sim \left(0,\ \sigma_w^2 \mathbf{I}_{N_r}\right)$, where $\sigma_w^2$ is the noise power or variance and $\mathbf{I}$ is square identity matrix of order $N_r$. So far, all the above given random variables are assumed uncorrelated and independent of each other.

The simplest STBC scheme, a $2 \times 2$ MIMO scheme, was first proposed by Alamouti, and later was relaxed to arbitrary multiple antennas in the context of general orthogonal designs [41], [42]. The design of an STBC code matrix $\mathbf{X}$ can be usually expressed as per the following linear relationship [24], [25], [37], [41], [42]:

$$\mathbf{X} = \sum_{m=1}^{M} \Re(s_m) \tilde{\mathbf{A}}_m + j\Im(s_m) \tilde{\mathbf{B}}_m \tag{4}$$

and by substituting $s_m = \Re(s_m) + j\Im(s_m)$ yields:

$$\mathbf{X} = \sum_{m=1}^{M} s_m \mathbf{A}_m + s_m^* \mathbf{B}_m \tag{5}$$

where a complex set of $M$ symbols is mapped onto a code matrix $\{s_1, s_2, \ldots, s_M\} \in \mathbf{S} \rightarrow \mathbf{X}$ using arbitrary basis matrices $\{\mathbf{A}_m, \mathbf{B}_m\}$, with $\mathbf{A}_m = (\mathbf{A}_m + \mathbf{B}_m)/2$ and $\mathbf{B}_m = (\mathbf{A}_m - \mathbf{B}_m)/2$ and all these matrices depend on the code design and have $N_t$ real entries, whereas $\Re(.)$ and $\Im(.)$ are the real and imaginary parts, and $(.)^*$ is the complex conjugate. The vector forms can now be defined below [24], [25], [37], [41], [42]:

$$\Re(\mathbf{S}) = \left[\Re(s_1) \ \ldots \ \Re(s_M)\right]^{\mathrm{T}}$$

$$\Im(\mathbf{S}) = \left[\Im(s_1) \ \ldots \ \Im(s_M)\right]^{\mathrm{T}}$$

$$\mathbf{S} = \left[\Re(\mathbf{S}) \ \Im(\mathbf{S})\right]^{\mathrm{T}} \tag{6}$$

and also:

$$\mathbf{F}_a = \left[\mathrm{vec}(\mathbf{H}\mathbf{A}_1) \ \ldots \ \mathrm{vec}(\mathbf{H}\mathbf{A}_M)\right]$$

$$\mathbf{F}_b = \left[j\left(\mathrm{vec}(\mathbf{H}\mathbf{B}_1)\right) \ \ldots j\left(\mathrm{vec}(\mathbf{H}\mathbf{B}_\mathbf{M})\right)\right]$$

$$\mathbf{F} = \left[\mathbf{F}_a \ \mathbf{F}_b\right] \tag{7}$$

which results in the following explicit form of space-time signal model relying on the actual information-bearing symbols:

$$\mathbf{Y} = \mathbf{F}\mathbf{S}^{\mathrm{T}} + \mathbf{W} \tag{8}$$

where vec(.) is a vector of stacking columns of the matrix argument (.), $\mathbf{F}$ is a generator matrix for the STBC code matrix $\mathbf{X}$, and $(.)^{\mathrm{T}}$ is the transpose operator, while the statistics of $\mathbf{W}$ do not change due to this transformation action.

A space-time matched filter (STMF) of the form $\mathbf{F}^*$ on the receiver side can easily retrieve the STBC signal model given in (5). This has the similar action of applying the maximum ratio combining (MRC) scheme to enhance the signal strength, and the signal can hence be straightforwardly recovered as below:

$$y_m(k) = \mathbf{F}^*\mathbf{Y} = \|\mathbf{H}\|_{\mathrm{F}}^2 s_m(k) + w_m(k), \ \nabla m \in [1, \ M] \tag{9}$$

Owing to the properties of $\mathbf{A}_m$ and $\mathbf{B}_m$, (9) can be easily verified since the squared Frobenius norm of $\mathbf{H}$ is given as $\|\mathbf{H}\|_{\mathrm{F}}^2 = \mathrm{Tr}(\mathbf{H}\mathbf{H}^*) = \sum_{n_r=1}^{N_r}\sum_{n_t=1}^{N_t}\left|h_{n_r n_t}\right|^2$, where Tr(.) is the trace operator. The above STBC linear processing has transformed the multipath fading channel to a set of $R = (N_t, N_r)$ independent parallel flat channels with coefficients $\|\mathbf{H}\|_{\mathrm{F}}^2$, symbols' variance is $\sigma_S^2$, while the white noise remains the same. The transformed channel has $\lambda = \|\mathbf{H}\|_{\mathrm{F}}^2 = \mathrm{diag}[\lambda_1, \ \lambda_2, \ \ldots, \ \lambda_R]$ eigenvalues, where $\lambda_r > 0$ is sorted in descending order $\lambda_r \geq \lambda_r + 1$. These eigenvalues are considered to be random variables of Chi-square distribution and $2N_tN_r$ degrees of freedom [43]. Reckoning (9) for each constellation symbol traversing through effective eigen channel paths:

$$y(k) = \sum_{m=1}^{M} \sum_{r=1}^{R} \lambda_r s_m(k) + w_m(k) \tag{10}$$

Meriting the orthogonality between the effective channel components is already inherited in the STBC structure; no further channel decomposition is needed. The above analysis appears idealistic by assuming perfect channel knowledge and timing between transmitter and receiver; however, it represents the upper bound on the detector performance. The assumptions of holistic channel knowledge and timing do not constitute any issue with the applicability of the given analysis. It is worth recalling that the IEEE 802.22 has warranted pilot signals at the beginning of each data frame that can be used for synchronization purposes [40]. Such signals help estimate the channel state information (CSI) using conventional estimation methods. The above analysis is considered valid under various situations unless otherwise different constraints are imposed.

## 4. Higher-order STBC

Alamouti code is widely known as the simplest STBC form with MISO antennas configured $N_t = 2$ and $N_r = 1$. For the binary phase shift keying (BPSK), the coding rate is $R$ = constellation size/STBC time interval = $M/(N_S = M) = 1$, and the full data rate is hence achieved with full diversity order. Alamouti code is represented by the following data and channel matrices [24], [37], [41], [42]:

$$\mathbf{X} = \mathbf{X}_{12} = \begin{bmatrix} s_1 & -s_2^* \\ s_2 & s_1^* \end{bmatrix}, \ \mathbf{H} = \mathbf{H}_{12} = \begin{bmatrix} h_1 & h_2 \end{bmatrix} \tag{11}$$

which can be converted to their STBC counterparts as follows:

$$\mathbf{S} = \begin{bmatrix} s_1 \\ s_2 \end{bmatrix}, \ \mathbf{F} = \begin{bmatrix} h_1 & h_2 \\ -h_2^* & h_1^* \end{bmatrix} \tag{12}$$

Several arbitrary higher-order STBC codes can be found in the literature. Most of the available codes were aimed to enable the highest possible diversity and coding gains, which can be obtained from MIMO channels. However, the rates cannot be higher than 1 symbol per channel use, which is the same situation for single-antenna systems [41], [42]. As an extension to the Alamouti code, possible combinations of symmetrical higher-order codes can be readily devised with 4 × 4 and 8 × 8 complex entries as in the following ABBA scheme for a code rate of 1 and full diversity order [44]:

$$\mathbf{X} = \begin{bmatrix} \mathbf{X}_{12} & -\mathbf{X}_{34}^* \\ \mathbf{X}_{34} & \mathbf{X}_{12}^* \end{bmatrix} \tag{13}$$

and:

$$\mathbf{X} = \begin{bmatrix} \mathbf{X}_{12} & -\mathbf{X}_{34}^* & -\mathbf{X}_{56}^* & \mathbf{X}_{78} \\ \mathbf{X}_{34} & \mathbf{X}_{12}^* & -\mathbf{X}_{78}^* & -\mathbf{X}_{56} \\ \mathbf{X}_{56} & -\mathbf{X}_{78}^* & \mathbf{X}_{12}^* & -\mathbf{X}_{34} \\ \mathbf{X}_{78} & \mathbf{X}_{56}^* & \mathbf{X}_{34}^* & \mathbf{X}_{12} \end{bmatrix} \tag{14}$$

Worth to mention is that, for complex constellations like $M$-ary quadrature amplitude modulation (MQAM) or $M$-ary phase shift keying (MPSK), STBC codes with a coding rate of 1 and full diversity order are unknown to exist or not for $N_t > 2$ antennas. Such codes, generally, are not believed to exist when the number of antennas $N_t$ equals the number of

both data symbols and time slots needed to transmit the code block [31], [41], [42].

## 5. MTM spectrum sensing and statistics

The MTSE employs a set of robust Slepian tapers of varying lengths to control the bias-variance trade-offs and maximize the spectral density within a desirable bandwidth $B$. The bandwidth is considered to be normalized by the sampling frequency in such analysis. Solving $\mathbf{R}\mathbf{v}_k = \psi_k \mathbf{v}_k$ generates the tapers, where $\mathbf{R}$ is the $K \times K$ positive-definite Toeplitz autocorrelation matrix, and the $(p, q)^{\text{th}}$ entry of this kernel matrix is defined by $R_{p,\,q} = \sin 2\pi B(p-q)/\pi(p-q)$ for $p, q = 1, 2, ..., K$ [21], [22], [45], [47]. The principle eigenvalues $\psi_k$ (or tapers) of the eigenvector $\boldsymbol{v}_k$, are ranged between 0 and 1 and ordered in a descending manner such that $\psi_0 \geq \psi_1 \geq \ \ldots \ \geq \psi_{K-1}$. The first $L \approx 2KB$ of these tapers are dominating, whereas the rest are of lesser effect. Moreover, the tapers of lower order have much stronger power concentration compared to the higher order tapers, therefore, signifying the first 3 to 6 of $L$ tapers for SE seem more realistic. Also, the $L$ value defines the degree of freedom (DoF) for controlling the SE variance.

The sum of weighted eigenspectrums (or power spectrum density PSD) of tapered data sequence in the frequency domain forms the MTSE as given below [21]-[23], [45], [47]:

$$\hat{S}_y(f) = \frac{\sum_{l=0}^{L-1} \psi_l \left|Y_l(f)\right|^2}{\sum_{l=0}^{L-1} \psi_l} = \sum_{l=0}^{L-1} \alpha_l \left|Y_l(f)\right|^2 \tag{15}$$

The weighting factors $\alpha_l = \psi_l / \left(\psi_0 + \ \ldots \ + \psi_{L-1}\right)$ represent another set of eigenvalues associated with each of the $l^{th}$ eigenspectrum. The term $\sum_{l=0}^{L-1} \psi_l$ represents the normalization factor and its total sum is 1, which can be discarded without impacting the decision-making. The fast Fourier transform (FFT) of the received data sequence for Slepian tapers $\{v_l\}_{k=0}^{K-1}$ and the corresponding PSD estimates are given below, respectively:

$$Y_l(f) = \frac{1}{K} \sum_{k=0}^{K-1} y(k) v_l(k) e^{-j2\pi fk} \tag{16}$$

$$\hat{S}_y(f) = \frac{1}{LK} \sum_{l=0}^{L-1} \sum_{k=0}^{K-1} \alpha_l \left| y(k) v_l(k) e^{-j2\pi fk} \right|^2 \tag{17}$$

For further simplification, let a new set of vectors be defined to exploit the quadratic matrix formation. Extending the approach of [24], [25], [45], [47], assume the following vector variables:

$$\mathbf{v}_l = \left[v_l(1),\ v_l(2),\ \ldots,\ v_l(K)\right]^{\mathrm{T}}$$

$$\mathbf{y} = \left[y(1),\ y(2),\ \ldots,\ y(K)\right]^{\mathrm{T}}$$

$$\mathbf{a} = \left[e^{j2\pi f},\ e^{j2\pi f 2},\ \ldots,\ e^{j2\pi fK}\right]^{\mathrm{T}} \tag{18}$$

where $\mathbf{b}_l = \mathbf{v}_l \odot \mathbf{a}$ and $\odot$ refers to the Hadamard product. Substituting (18) in (16) reveals $Y_l(f) = \mathbf{b}_l^{\dagger} y$, which, when used together with the Slepian tapers, will alter (17) to have the PSD estimate of quadrature form approximation below:

$$\hat{S}_y(f) = \mathbf{y}^{\dagger} \boldsymbol{\Omega} \mathbf{y} \tag{19}$$

where $\boldsymbol{\Omega}$ is the $L \times L$ idempotent matrix defined as $\boldsymbol{\Omega} = \sum_{l=0}^{L-1} \alpha_l \mathbf{b}_l \mathbf{b}_l^{\dagger}$ and $(.)^{\dagger}$ is the Hermitian operator, The above PSD

is a scalar expression, which can be viewed as the sum of individual PSDs calculated over dominant tapers. Note that the inverse FFT order is purposely assumed equivalent to the data sequence length for ease of manipulation and to avoid adverse computations in the simulation results section.

## 6. Hypothesis test

The binary hypothesis test (BHT) realizes the statistical decision policy in this study. There are two main observations, $\mathcal{H}_0$ and $\mathcal{H}_1$ intended to differentiate between the idle and active states of a PU. When a PU is present and active, the observation $\mathcal{H}_1$ is applicable, while vice versa is true for the absent and idle state. Two corresponding probabilities are thus essential: the probability of correct detection $P_D$ and the probability of false alarm $P_{FA}$. In the framework of NP optimal criterion and given a sufficient test statistic defined in terms of $\hat{S}_y(f)$, the probabilities defined by:

$$P_{FA} = \Pr\left\{\hat{S}_y(f) > \eta |\ \mathcal{H}_0\right\}$$

$$P_D = \Pr\left\{\hat{S}_y(f) > \eta |\ \mathcal{H}_1\right\} \tag{20}$$

where $\eta$ is a threshold determined concerning the required constant false alarm rate (CFAR). The CFAR method is common in practice and used when the test statistic and the optimal threshold are unaffected by scaling the received sequence and when the power of observation noise is unknown [12]. The summation of channel eigenvalues can be assumed to be 1, and the central limit theory (CLT) is applicable here given a large set of data sequences [43]. Tracing back the received sequence into its original constellation and the effective channel eigenvalue components reduces the BHT decision statistics to take the following form, which is readily approximated after summing and averaging concerning all constant parameters [24]:

$$\text{Decide: } \mathcal{H}_0 \text{ if } \hat{S}_y(f) \approx^{\text{d}} \sigma_w^2 \chi^2_{RMLK}$$

$$\text{Decide: } \mathcal{H}_1 \text{ if } \hat{S}_y(f) \approx^{\text{d}} \left(\sigma_s^2 + \sigma_w^2\right) \chi^2_{RMLK} \tag{21}$$

where $\approx^{\text{d}}$ stands for "equal in distribution", $\sigma_S^2$ is the signal power or variance and the normal variables are attributed to the CLT convergence into Chi-square distribution while passing through Rayleigh channels. The probability asymptotes given in [32], [33] can be worked out to reflect on the new MTSE-STBC parameters' contribution to yield [24]:

$$P_{FA} = Q\left\{\frac{\eta - RMLK\sigma_w^2}{2\sigma_w^2\sqrt{RMLK/2}}\right\}$$

$$P_D = Q\left\{\frac{\eta - RMLK\left(\sigma_s^2 + \sigma_w^2\right)}{2\left(\sigma_s^2 + \sigma_w^2\right)\sqrt{RMLK/2}}\right\} \tag{22}$$

where Q(.) is the right tail cumulative distribution function, and the expression *RMLK* symbolizes the multiplication of variables of the designated spaces. Rearranging the above two probabilities in terms of the $SNR = \sigma_s^2/\sigma_w^2$ and new threshold $\dot{\eta} = \eta/\sigma_w^2$ simplifies the expressions as below:

$$P_{FA} = \mathrm{Q}\left\{\frac{\acute{\eta} - RMLK}{2\sqrt{RMLK/2}}\right\}$$

$$P_{D} = \mathrm{Q}\left\{\frac{\acute{\eta} - RMLK(SNR+1)}{2(SNR+1)\sqrt{RMLK/2}}\right\} \tag{23}$$

The above approximation considers the broad concept of having the natural noise perturbation vary almost within a certain extent in a knowingly fixed environment and hence stationary. The signal power is relative to the distance between the SU receiver and the PU transmitter [7], [8]. The signal power is difficult to estimate as it changes depending on ongoing transmission characteristics and the distance between the CR and PU terminals [10]. Otherwise, in the worst-case scenario, the noise power can be adaptively estimated and compensated and hence it remains for the signal power variations through the *SNR* figure to act as a crucial performance indicator. Worth mentioning is that, it has been demonstrated that in most of the investigated SE technologies, apart from ED, the noise variance uncertainty does not affect their relative performances as they exhibit similar robustness to noise variance uncertainty [30]. Such robustness can also be generally ratified over the MTSE method [21]-[23].

# 7. Threshold adaptation

## 7.1 *Threshold criterion*

Before delving into the threshold adjustment analysis, let us examine the signaling statistics first. Two situations are worth noting as can be observed in Figure 2. Although a zero mean noise is normally applicable in both situations, the signal sequence may tell a different story. This is largely pertinent to the signaling scheme being used for transmission, which can be either of zero means or not irrespective of variance (or power). Part (Up) of Figure 2 provides a statistical behavior commonly reflected by many studies in the literature. Despite the signal appearing to have a non-zero mean value, however, an elaboration on such a stance is almost dismissed in many studies, such as in [13]. It is notoriously known that the realism of such a situation is of practical limitations, as signaling of non-zero means does not meet certain transmission and processing design requirements. The signal and noise variances could be different.

Furthermore, part (Up) of Figure 2 also portrays the false alarm $P_{FA}$ and the miss detection of $P_{MD} = 1 - P_{D}$ probabilities and how they can be controlled by threshold adjustment. The typical purpose of most SE techniques is to reduce these two probabilities, as best as possible. However, this cannot be easily accomplished as these two probabilistic entities behave independently. Stretching the threshold value up or down will have a tandem effect on the PU protection and efficient spectrum utilization, whether favorably or not. A trade-off is therefore essential in such situations, subject to the SE design and performance measures.

On the other hand, part (Down) of Figure 2 seems more realistic. It shows zero mean values for both the signal and noise which is a fair resemblance to practical conditions. They differ only in variances. Imagine a statistical distribution is trended to emulate the threshold, and such trend lies between the other two belonging to signal and noise as shown in the same figure. The interpretation of increasing or decreasing threshold on the probabilities metrics applies exactly as described above. It is imperative to assert that the analysis and derivations given in this work apply equally to both parts of Figure 2. The *SNR* can further unravel this issue as demonstrated below.

The *SNR* value has a radical influence on $P_{D}$, or $P_{MD}$, while the $P_{FA}$ can be changed by the noise variance only and hence can be fixed to any desired value independently from $P_{MD}$. The orthogonal STBC decouples the spatiotemporal channel into parallel and independent scalar channels each with *SNR* expressed as follows [41], [42]:

$$SNR = \frac{\mathbb{E}\left[\mathrm{Tr}\left(\mathbf{H}\mathbf{X}\mathbf{X}^{\dagger}\mathbf{H}^{\dagger}\right)\right]}{\mathbb{E}\left[\mathrm{Tr}\left(\mathbf{W}\mathbf{W}^{\dagger}\right)\right]} \tag{24}$$

Recall that $\mathbb{E}\left[\mathrm{Tr}\left(\mathbf{XX}^{\dagger}\right)=\mathbb{E}\left[\|\mathbf{S}\|^{2}\right]\right]$, $\mathbb{E}\left[\mathrm{Tr}\left(\mathbf{HH}^{\dagger}\right)=\mathrm{Tr}\left(\mathbf{FF}^{\dagger}\right)=\mathbb{E}\left[\|\mathbf{H}\|^{2}\right]\right]$, and $\mathbb{E}\left[\mathrm{Tr}\left(\mathbf{WW}^{\dagger}\right)\right]=\sigma_{w}^{2}$ [41], [42]. After normalization and omission of scalars, (24) is reduced to:

$$SNR=\frac{\left(\mu_{s+}^{2}\sigma_{s}^{2}\right)}{\sigma_{w}^{2}} \tag{25}$$

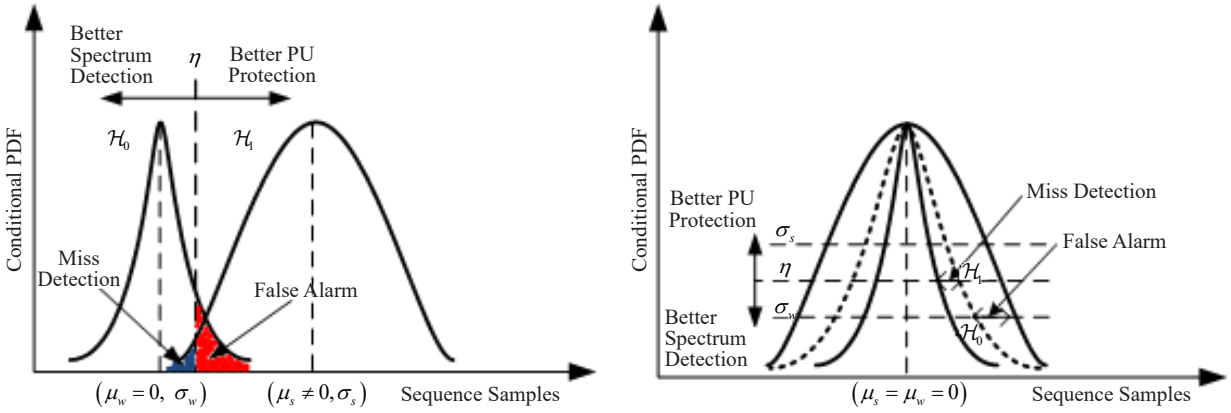


**Figure 2.** Signal statistics: (Up) Mean value not equal to zero; (Down) Mean value equal to zero

This clearly shows the link between the first two statistical moments and the STBC signal power design, as was generalized in both parts of Figure 2. Therefore, articulating the actual statistical behavior of the signal and noise attributes and their contribution to analysis can be proved instructive and cannot be merely undeclared. Hence, it is important to reiterate that the discussion of MTSE-STBC offered in this work is still applicable whether the signal has an average value of zero or not.

## 7.2 *Threshold adjustment*

Conventional SE designs are generally based on either the CFAR or constant detection rate (CDR) performance measures, where the first is described earlier in the context and the second relates to $P_D$ exclusively. The CFAR maintains better spectrum reuse, while the CDR provides better protection for PUs against undesirable interferences from unknown sources or intruders. Constant performance indicators can be produced by both methods irrespective of the SNR or noise power variations. To be more rewarding for both PUs and SUs, a threshold adjustment methodology needs to be appropriately devised to achieve the best trade-off optimization between $P_D$ and $P_{FA}$ under different work scenarios.

Some studies revealed the weighted trade-off principle (WTP) to minimize the decision error probability of SE [23], [25], [32], [33], which will also be adopted here. The optimum threshold value has to be selected to minimize the following convex function of total error decision probability:

$$P_E=\alpha P_{FA}+(1-\alpha)P_{MD} \tag{26}$$

where the trade-off is formed between the probability of a false alarm relative to that of missed detection can be attained concerning a predefined weighting, or spectrum utilization, factor, within the range $0<\alpha<1$. Substituting (23) in (26) yields:

$$P_E=\alpha Q\left\{\frac{\acute{\eta}-RMLK}{2\sqrt{RMLK/2}}\right\}+(1-\alpha)\left(1-\mathrm{Q}\left\{\frac{\acute{\eta}-RMLK(SNR+1)}{2(SNR+1)\sqrt{RMLK/2}}\right\}\right) \tag{27}$$

The minimization of the above formula can be done by taking the first derivative of (27) concerning $\acute{\eta}$ and making it equal to zero subject to the second derivative being greater than zero. After substituting $\mathrm{Q(z)} = \frac{1}{2\pi}\int_{z}^{\infty} \mathrm{e}^{-\frac{t^2}{2}}\mathrm{d}t$ and rearranging, this will reduce to the quadrature equation below:

$$\frac{(SNR+2)}{2(SNR+1)}\acute{\eta}^2 - \sigma_w^2\acute{\eta} - \frac{2\sigma_w^2(SNR+1)}{RMLK\cdot SNR}\ln\left\{\frac{\alpha}{(1-\alpha)}(SNR+1)\right\} = 0 \tag{28}$$

and solving for the positive threshold yields:

$$\acute{\eta} = \frac{1+\sqrt{1+\frac{4}{RMLK}\left(1+\frac{2}{SNR}\right)\ln\left(\frac{\alpha}{(1-\alpha)}(SNR+1)\right)}}{(SNR+2)/(SNR+1)} \tag{29}$$

As *RMLK* tends to have a large value near infinity, this was suggested to be approximated as [32]:

$$\acute{\eta} \approx 2(SNR+1)/(SNR+2) \tag{30}$$

A value in the range of $RMLK \approx 100$ and higher can be considered fairly sufficient for the above asymptote to be applicable. The last two expressions illustrate that the threshold value is largely determined by the *SNR* variations and hence an adequate adaptation policy needs to be explored further. The above derivations are given by one threshold setting only. This is commonly known in the literature as a one-stage adaptive threshold. Other studies also advocate more than one-stage threshold schemes [8], [34].

## 8. Simulation results

In this section, numerical simulations are presented to corroborate the viability of the above theoretical analysis. Selecting an appropriate range of Slepian tapers is first explored because it directly impacts the computational bearing. The trend of various Slepian tapers is illustrated in Figure 3 using 6 tapers and a half-time-bandwidth product *KB* equal to 0.0625 and 1, respectively. The number *KB* = 1, or DoF, is distinctive since it identifies the broader line between low and rapid amplitude fluctuations of such tapers. This will accordingly constitute more number tapers to be accounted for their energy congregates.

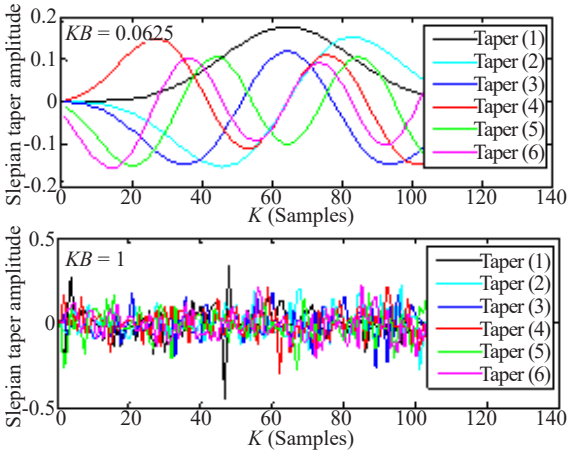


**Figure 3.** Representation of 6 Slepian Tapers with two different *KB* values: (Up) *KB* = 0.0625; (Down) *KB* = 1

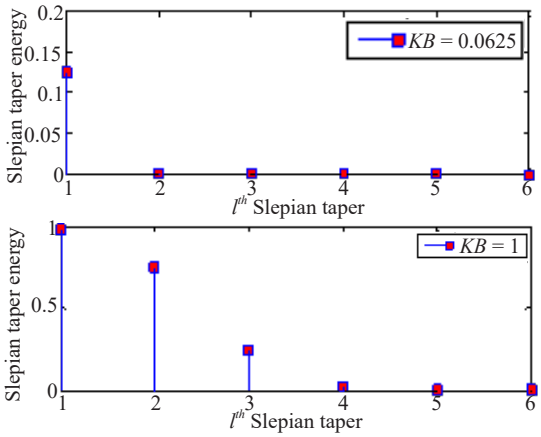


**Figure 4.** Energy concentration of 6 Slepian Tapers with two different *KB* values: (Up) *KB* = 0.0625; (Down) *KB* = 1

It is evident from Figure 4 that increasing the number of tapers would not be rewarding for the MTSE algorithm because most of the effective energy is focused on the low-order tapers. These lower-order tapers impose greater control on the spectrum bias, and the opposite is true for the higher-order tapers. The behavior of Slepian tapers acts as a bandpass filter, as given in equations (15)-(17), and thus delivers sharp spectrum truncation and better smoothing. Increasing the number of tapers will have energy dispersed over many orthogonal elements. As the half multiplier of time-bandwidth increases from 0.0625 to 1, the tapers eventually develop more erratic behavior as lots of energy shifts to the higher-order tapers.

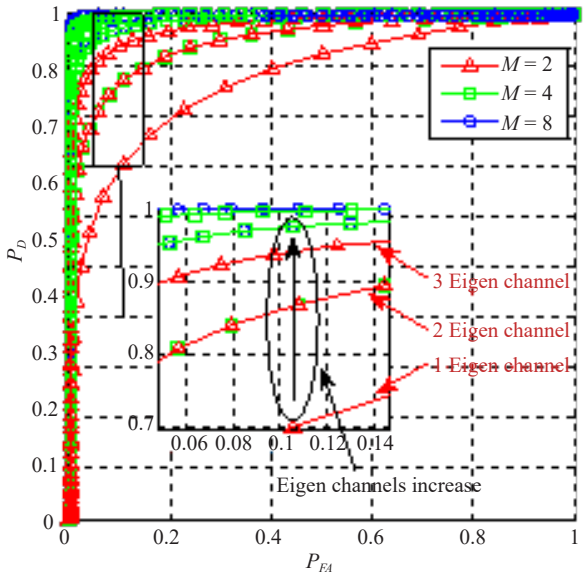


**Figure 5.** ROC of MTSE-STBC against *M*-ary and STBC order variations

An important tool in the performance evaluation of a detector is called the receiver operation characteristic (ROC), which represents the relationship between the two probabilities described in (22) or (23). By varying the threshold $\eta$, or $\acute{\eta}$, the operating point of a detector can be chosen anywhere along its ROC curve. In the first example, 3 Slepian tapers are simulated in conjunction with *M*-ary constellations of 2, 4, and 8, which stand for BPSK, QPSK, or QAM, and 8-PSK

or 8-QAM, respectively. The *SNR* was set to 0 dB and the resulting ROC trend is portrayed in Figure 5. It shows that an improved performance can be gained by increasing the constellation size. It is important to note that the constellation size replicates the number of dominant eigenvalues, or parsed parallel paths, of an effective wireless channel regardless of coding gain. The larger the number of discriminated channels in a higher-order STBC scheme, the better detection performance could be attained.

The second exercise is on experimenting with a random sequence of 1,024 BPSK symbols sampled at $10^6$ Hz. Three Alamouti-based STBC configurations of 2 × 2, 4 × 4, and 8 × 8 are considered for transmission. The channel is designed to be a flat-fading Rayleigh with additive white Gaussian noise (AWGN) of zero mean and unit variance. On the receiver side, the incoming baseband sequence is independently admitted to the SE stage using two algorithms namely; the MTSE and Periodogram SE (PSE). The performances of these two SE algorithms are compared against each other to evaluate their detection accuracy concerning *SNR* variations in the range from -30 dB to 30 dB. The prefixed threshold values assumed a CFAR of 0.01 and CDR of 0.99 in each simulation setting. These values are commonly adopted and lie within the maximum acceptable range of 0.1 for $P_{FA}$ and $P_{MD}$ as defined in the IEEE 802.22 regulation [7], [12], [27]. A Monte Carlo of $10^5$ repetitions is applied and the resulting values of probability of error sensing, or false alarm, against the *SNR* increment are shown in Figure 6.

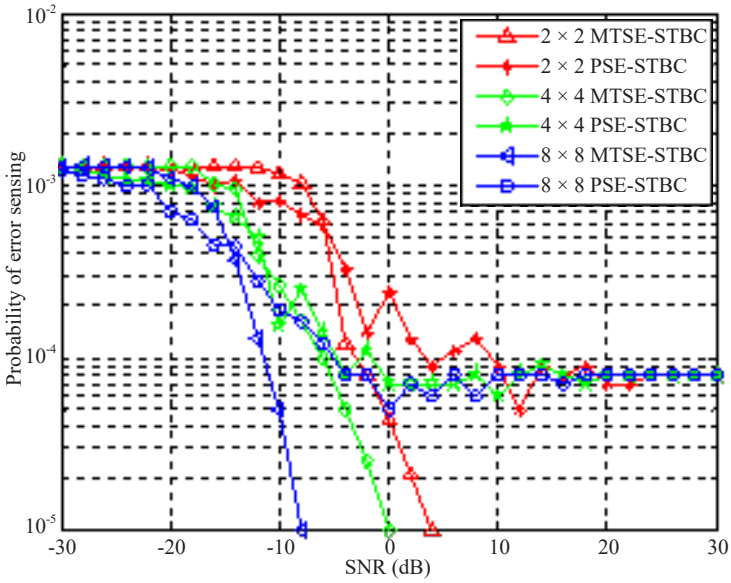


**Figure 6.** Probability of error sensing of MTSE-STBC and PSE-STBC against *SNR* variations

It is evident from Figure 6 that diminishing values of error probabilities are obtained when the *SNR* increases beyond 0 dB in the case of the MTSE methodology. Even rapidly falling values are noticeable for higher-order STBC schemes, which are considered a favorable trend indicating performance improvement. The same behavior is encountered in the case of PSE as also shown in Figure 6, however, such speedily declining values are now of less encounter. This can be attributed to having no control over the noise amount entering a particular bandwidth upon which the detection process is implemented. Opposite to the PSE inactive behavior, the MTSE leverages stringent control on the noise affecting the desirable bandwidths and thus produces robust spectrum detection results. It is therefore quite apparent from the trend of this figure that as the STBC order increases (or equally the *M*-ary and MIMO sizes), the better spectrum detection is attained. This is irrespective of coding gain, which is not the focus of this study and could be occasionally sacrificed in particular situations. Most remarkably, the MTSE outperforms the PSE for the same test settings an extension of which can be intuitively generalized over other practical situations.

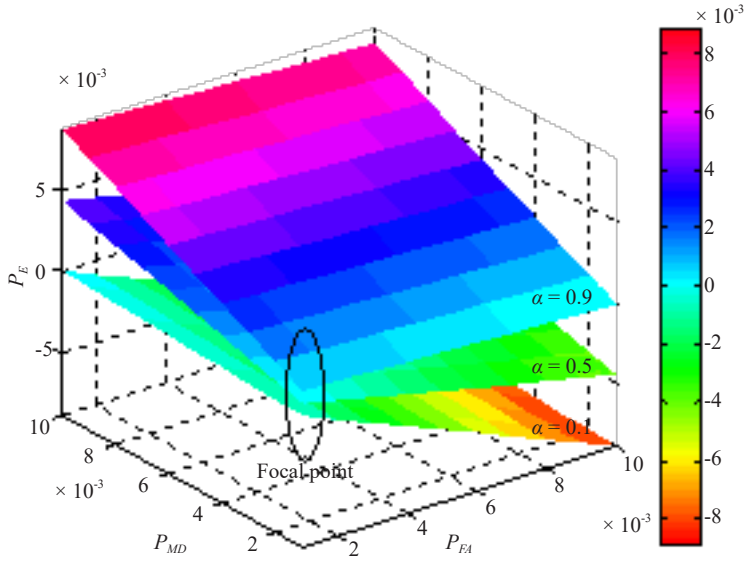


**Figure 7.** Total error probability concerning $P_{FA}$ and $P_{MD}$ variations and selected values of utilization factor $\alpha$

The threshold requirement is now examined. The convex optimization problem given in (26) is first assessed as illustrated in Figure 7. The values of $P_{FA}$ and $P_{MD}$ are varied within admissible ranges meeting the functional requirements outlined in IEEE 802.22 and stated above in the context. While, on the other hand, three different arbitrary values are selected for the utilization factor $\alpha = 0.1$, 0.5, and 0.9. As intuitively depicted in Figure 7, the convex function represents a linear relationship of two-variable planes. The utility factor governs the orientation of such planes, but apparently, all planes coincide at one point in which the value of $P_E$ reaches 0. When the convex formula is optimized properly, it will produce the required threshold at the shown focal point, which makes the $P_E$ value equals 0 and minimizes $P_{FA}$ and $P_{MD}$ irrespective of the utilization parameter. One might wonder about the negative values of $P_E$, which is merely a theoretical result and has no meaning in reality and can be dismissed accordingly.

The detection threshold behavior is secondly assessed for the same arbitrary utilization factors mentioned above and as shown in Figure 8. Three trends are consequently generated for each utilization factor as per the expression in (29), and the fourth trend reflects on the asymptotic threshold behavior given in (30). The number of points in the processing window is 12,288 as the minimum (equivalent to a BPSK sequence of 1,024 samples) and applied to 2-order STBC and 3 Slepian tapers for the MTSE. This number surely increases as the complexity of *M*-ary and STBC sizes climb while keeping the same number of sample points. Therefore, the asymptotic approximation condition given in (30) is assumed to be met.

Figure 8 clearly illustrates that the asymptotic threshold trend is perfectly aligned with the threshold trend allocated for the utilization factor of $\alpha = 0.5$, which will be called threshold couples here. This coincides with the results of the same situation provided in [32]. That means the asymptotic threshold behavior resembles that of $\alpha = 0.5$, which is borderline to differentiate between two preferences of efficient spectrum reuse or PUs protection requirements. Both trends of threshold couples, and irrespective of *SNR* values, separate the remaining trends of $\alpha > < 0.5$ into two symmetrical zones. The threshold trends of $\alpha < 0.5$ are aimed for better spectrum reuse lying above the threshold couples, while the opposite is true aimed for better PUs protection of $\alpha > 0.5$. The analysis and results of this paper largely match those given in [32], however, it is worth learning about the slightly mismatched interpretation of $\alpha$ in both. Due to $\alpha$ in (26) and (29) being allocated differently to Eqs. (6) and (11) of [32], the lower and higher $\alpha$ bounds means are exactly the opposite in terms of spectrum reuse and PUs preferences. Aside from that and more interestingly, the $\alpha$ compilation of this work is a compatible match with that given in Eqs. (9) and (12) of [32]. Therefore, the representations provided in this paper are appealed to be accurately more persuasive in comparison to other results given elsewhere.

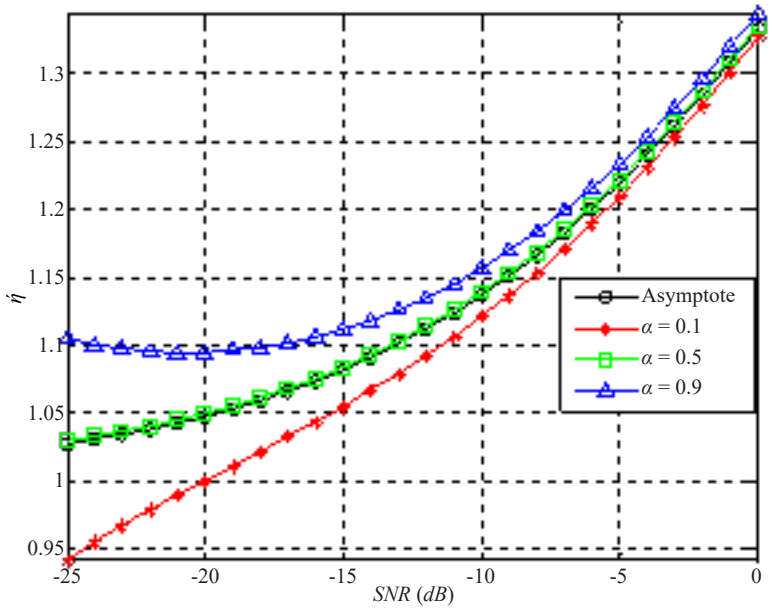


**Figure 8.** Detection threshold against *SNR* variations: asymptote and selected values of utilization factor $\alpha$

Two distinct observations in Figure 8 are also worthy of further attention. The first one is pertinent to the threshold performance for *SNR* values larger than 0 dB, while the second one relates to *SNR* values smaller than 0 dB. Regardless of the utilization factor, the threshold couples and other trends show almost similar inclinations for larger *SNR* values. This means the received *SNR* value is relatively large enough to retain spectrum reuse and PUs protection equally balanced without major efforts. However, smaller *SNR* values entail greater thresholds for better PU protection when the fixed value of $\alpha$ is small. Otherwise, for larger $\alpha$ and smaller *SNR* values, the threshold values decrease to allow for better spectrum reuse. Therefore, an adaptive SE can be intuitively administered by knowing the *SNR* value and window processing length. Such adaptation can be attended as per (29), the result of which is substituted in (27) for predefined probability metrics and spectrum utilization determined in (26).

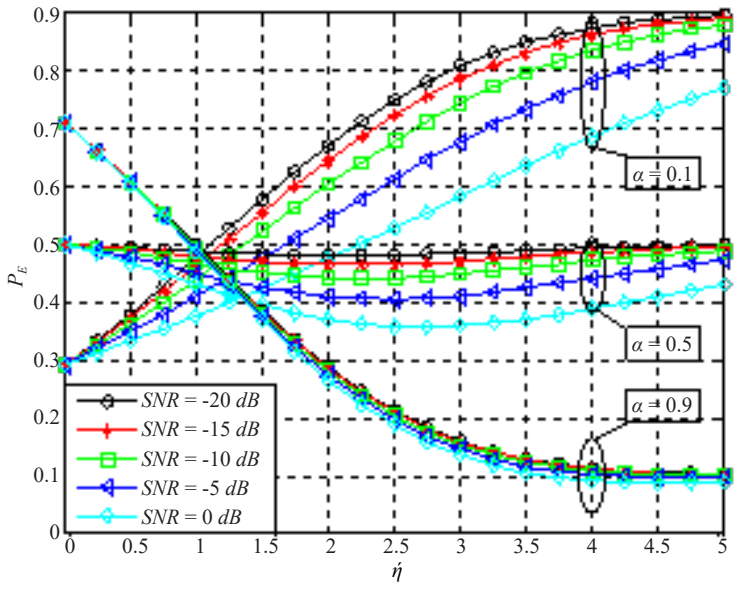


**Figure 9.** Probability of error against normalized threshold variations: selected values of *SNR* and utilization factor $\alpha$

The $P_E$ versus normalized threshold values and concerning particular values of *SNR* (-20 dB, -15 dB, -10 dB, -5 dB, and 0 dB) and utilization factor $\alpha$ (0.1, 0.5, and 0.9) are depicted in Figure 9. This can be envisaged as a 2D representation of the $P_E$ shown above in Figure 8 but now adhered to threshold, *SNR*, and utilization factor variations. The convex function behavior is well discerned for a 0.5 utilization factor. This means detecting a spectrum void or protecting the presence of a PU is of equal preference. The $P_E$ is not expected to exceed 0.5 at best in such a situation, whereas values of the optimum threshold can be examined and adjusted as desirable as can be seen in the same figure. As can be seen from Figure 9, the situation of allocating more PU protection or insisting on occupying void spectrum holes would result in different trends getting away from the convex dwelling center points. Both performances of protecting a PU and reusing the available spectrum voids can be mainly improved by enhancing the *SNR* at the front-end receiver. This can also be achieved by manipulating the threshold optimization as well. On the other hand, the value 0.9 of the utilization factor demonstrates an inverse exponential that rapidly drops indicating more protection for a PU is gained when threshold values increase. However, the $P_E$ values always start at 0.7 when the threshold value is zero regardless of the *SNR* under such a scenario. Larger threshold values mean having more confidence that a PU is not present and the $P_E$ improves accordingly. The adverse of such behavior occurs by having smaller threshold values which means focusing more on occupying a spectrum void at any price regardless of a PU presence. The $P_E$ values of such behavior always start at 0.3 when the threshold value is zero and dramatically deteriorate as threshold values increase. Such a situation indicates that no concern is exercised regarding a PU status. Such a scenario is seriously harmful and imposes constraints on the general utilization of the permissible useful spectrum range.

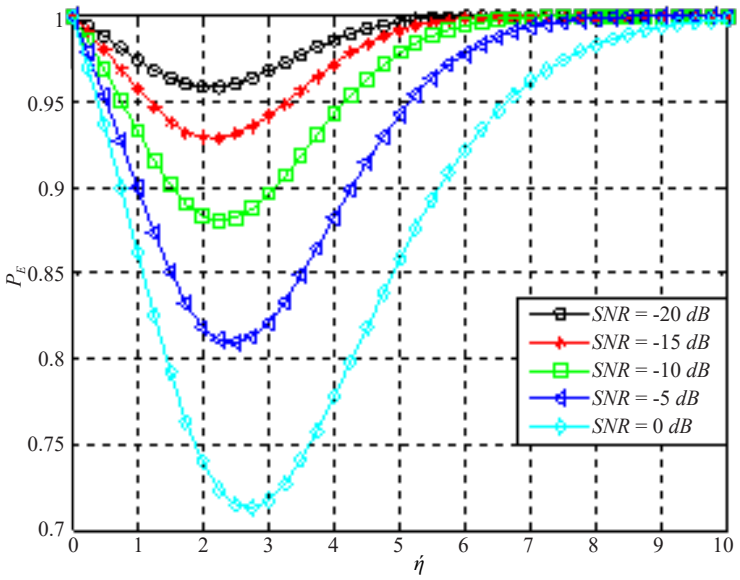


**Figure 10.** Probability of error concerning varying normalized threshold: selected values of SNR

The scenario of not using an appropriate utilization factor takes a rather different behavior as shown in Figure 10. It can be seen in this figure that the $P_E$ takes on different values from 1, going down to the dwelling minimum points of the convex curvature as per each *SNR*, and then climbing up to reach 1 again. This is fairly expected as there is no sense whatsoever of PUs' presence and hence $P_E$ may drastically deteriorate if not linked to properly selected optimum threshold values. The identification and selection of appropriate optimum threshold values plays a major role in such situations as shown in Figure 10. The dwelling minimum points also vary broadly as per variations in the *SNR* values, which was also fairly demonstrated in Figure 10 for the utilization factor $\alpha$ equal to 0.5, but the difference here is that the $P_E$ cannot reach the value of 1 under any circumstances due to the equal weighting of both probabilities contributing to the calculation of the overall $P_E$ in Figure 9. Better *SNR* values also contribute to improving the selection of optimum

threshold values, and this would hence result in better overall $P_E$ performances. Worth noting is that the trends of Figure 10 here have some similarities compared to the trends of (Figure 7 in [34]), however, a double thresholding scheme was considered in that study, which is not attempted in this paper.

## 9. Conclusion

A systematic paradigm by coupling the non-parametric MTM and higher-order STBC structures is developed, which is dubbed MTSE-STBC. The closed-form performance expressions are devised under flat-fading Rayleigh and AWGN channels. The statistical approximation asymptotes are derived considering predefined CFAR and CDR settings to adjust for an appropriate one-stage detection threshold. It is found that amending the threshold value is highly governed by the  parameter, especially when the processing window gets to a fairly large extent. Such processing window can be interpreted in dependence on the multiplication of the Slepian tapers, sequence sample length, number of multiple antennas, and constellation size. The latter two parameters are set to be equivalent to the STBC order in this article, whereas dissimilar situations can also be met somewhere else in the literature. Further manipulation of threshold adaptation is via augmenting utilization factors. Utilization factors larger than 0.5 enhance PU's protection and retain the detection of spectrum holes can be determined with better confidence. Utilization factors smaller than 0.5 render easier access to spectrum holes with less regard for PU's existence, and this would be at the expense of poorer PU's protection. If there is no intention to adopt utilization factors, then error probabilities can only be improved by relying on threshold values that are to be selected carefully.

The detection behavior is assessed using numerical computations. Results demonstrate that major performance boosts can be achieved by having higher-order STBC schemes aiming to retain space diversity regardless of coding gain. Importantly, the spatiotemporal orthogonality feature in the core of complex STBC structures is to be kept intact. Simulation exercises revealed improved performance compared to higher-order STBC schemes augmented to other SE algorithms like the Periodogram. Such improvement can be chiefly attributed to the Slepian tapers causing better spectrum windowing. The MTSE is deduced to be more resilient in controlling the leaking spectrum and produces better detection rates in the sub-bands of interest. The higher the STBC order, or MIMO structures, the better spectrum detection is achieved. The MTSE-STBC can also be generalized for other fading and selective channels using the same conceptual derivations presented in this paper.

## Conflict of interest

The authors declare that they have no conflict of interest.

## References


[1] D. Raychaudhuri and N. B. Mandayam, "Frontiers of wireless and mobile communications," *Proceedings of the IEEE*, vol. 100, no. 4, pp. 824-840, 2012.

[2] Y. C. Liang, K. C. Chen, G. Y. Li, and P. Mähönen, "Cognitive radio networking and communications: An overview," *IEEE Transactions on Vehicular Technology*, vol. 60, no. 7, pp. 3386-3407, 2011.

[3] J. Wang, M. Ghosh, and K. Challapali, "Emerging cognitive radio applications: A survey," *IEEE Communications Magazine*, vol. 49, no. 3, pp. 74-81, 2011.

[4] E. Hossain, D. Niyato, and D. I. Kim, "Evolution and future trends of research in cognitive radio: A contemporary survey," *Wireless Communications and Mobile Computing*, vol. 15, no. 11, pp. 1530-1564, 2015.

[5] A. Gupta and R. K. Jha, "A survey of 5G network: Architecture and emerging technologies," *IEEE Access*, vol. 3, pp. 1206-1232, 2015.

[6] M. Agiwal, A. Roy, and N. Saxena, "Next generation 5G wireless networks: A comprehensive survey," *IEEE Communications Surveys & Tutorials*, vol. 18, no. 3, pp. 1617-1655, 2016.

[7] R. Tandra, S. M. Mishra, and A. Sahai, "What is a spectrum hole and what does it take to recognize one?" *Proceedings of the IEEE*, vol. 97, no. 5, pp. 824-848, 2009.

[8] J. Ma, G. Y. Li, and B. H. Juang, "Signal processing in cognitive radio," *Proceedings of the IEEE*, vol. 97, no. 5, pp. 805-823, 2009.
[9] S. Senthilmurugan and T. G. Venkatesh, "Optimal channel sensing strategy for cognitive radio networks with Heavy-tailed idle times," *IEEE Transactions on Cognitive Communications and Networking*, vol. 3, no. 1, pp. 26-36, 2017.
[10] T. Yucek and H. Arslan, "A survey of spectrum sensing algorithms for cognitive radio applications," *IEEE Communications Surveys and Tutorials*, vol. 11, no.1, pp. 116-130, 2009.
[11] B. Wang and K. Liu, "Advances in cognitive radio networks: A survey," *IEEE Journal of Selected Topics in Signal Processing*, vol. 5, no. 1, pp. 5-23, 2011.
[12] E. Axell, G. Leus, E. G. Larsson, and H. V. Poor, "Spectrum sensing for cognitive radio: State of the art and recent advances," *IEEE Signal Processing Magazine*, vol. 29, no. 3, pp. 101-116, 2012.
[13] R. Umara and A. U. H. Sheikh, "A comparative study of spectrum awareness techniques for cognitive radio oriented wireless networks," *Physical Communication*, vol. 9, pp. 148-170, 2013.
[14] Y. Zeng, Y. C. Liang, A. T. Hoang, and R. Zhang, "A review on spectrum sensing for cognitive radio: Challenges and solutions," *EURASIP Journal on Advances in Signal Processing*, vol. 2010, pp. 1-15, 2010.
[15] H. Elshafie, N. Fisal, M. Abbas, W. A. Hassan, H. Mohamad, N. Ramli, S. Jayavalan, and S. Zubair, "A survey of cognitive radio and tv white spaces in malaysia," *Transactions on Emerging Telecommunications Technologies*, vol. 26, no. 6, pp. 975-991, 2015.
[16] N. Gul, M. S. Khan, S. M. Kim, J. Kim, A. Elahi, and Z. Khalil, "Boosted trees algorithm as reliable spectrum sensing scheme in the presence of malicious users," *Electronics*, vol. 9, no. 6, pp. 1038, 2020.
[17] R. S. Koteeshwari and B. Malarkodi, "Spectrum sensing techniques for 5G wireless networks: Mini review," *Sensors International*, vol. 3, pp. 100188, 2022.
[18] C. Pablos, A. G. Andrade, and G. Galaviz, "Modulation-agnostic spectrum sensing based on anomaly detection for cognitive radio," *ICT Express*, vol. 9, no. 3, pp. 398-402, 2023.
[19] S. Kim, "Multi-agent learning and bargaining scheme for cooperative spectrum sharing process," *IEEE Access*, vol. 11, pp. 47863-47872, 2023.
[20] A. Jain, N. Gupta, and M. Sreenu, "Blockchain based smart contract for cooperative spectrum sensing in cognitive radio networks for sustainable beyond 5G wireless communication," *Green Technologies and Sustainability*, vol. 1, no. 2, pp. 100019, 2023.
[21] S. Haykin, D. J. Thomson, and J. H. Reed, "Spectrum sensing for cognitive radio," *Proceedings of the IEEE*, vol. 97, no. 5, pp. 849-877, 2009
[22] S. Haykin, "Cognitive radio: Brain-empowered wireless communications," *IEEE Journal on Selected Areas in Communications*, vol. 23, no. 2, pp. 201-220, 2005.
[23] E. S. Hassan, "Adaptive threshold to guarantee both detection and false alarm probabilities in multi-taper based spectrum sensing," *Journal of the Franklin Institute*, vol. 356, pp. 1640-1657, 2019.
[24] A. O. Abdul Salam, R. E. Sheriff, S. R. Al-Araji, K. Mezher, and Q. Nasir, "Multi-taper spectrum-based estimator for cognitive radio using multiple antennas and STBC techniques," *IET Circuits, Devices & Systems*, vol. 12, no. 2, pp. 133-143, 2018.
[25] A. O. Abdul Salam, R. E. Sheriff, S. R. Al-Araji, K. Mezher, and Q. Nasir, "Adaptive threshold and optimal frame duration for multi-taper spectrum sensing in cognitive radio," *ICT Express*, vol. 5, no. 1, pp. 31-36, 2019.
[26] J. Mietzner, R. Schober, L. Lampe, W. H. Gerstacker, and P. A. Hoeher, "Multiple-antenna techniques for wireless Communications-A comprehensive literature survey," *IEEE Communications Surveys and Tutorials*, vol. 11, no. 2, pp. 87-105, 2009.
[27] R. Zhang, T. J. Lim, Y. C. Liang, and Y. Zeng, "Multi-antenna based spectrum sensing for cognitive radios: A GLRT approach," *IEEE Transactions on Communications*, vol. 58, no. 1, pp. 84-88, 2010.
[28] M. Al-Amidie, M. Al-Asadi, A. J. Humaidi, A. Al-Dujaili, L. Alzubaidi, L. Farhan, M. A. Fadhel, R. G. McGarvey, and N. E. Islam, "Robust spectrum sensing detector based on MIMO cognitive radios with non-perfect channel gain," *Electronics*, vol. 10, no. 529, pp. 1-19, 2021.
[29] E. Soltanmohammadi, M. Orooji, and M. Naraghi-Pour, "Spectrum sensing over MIMO channels using generalized likelihood ratio tests," *IEEE Signal Processing Letters*, vol. 20, no. 5, pp. 439-442, 2013.
[30] S. Sedighi, A. Taherpour, S. Gazor, and T. Khattab, "Eigenvalue-based multiple antenna spectrum sensing: Higher order moments," *IEEE Transactions on Wireless Communications*, vol. 16, no. 2, pp. 1168-1184, 2017.
[31] D. Gesbert, M. Shafi, D. Shiu, P. J. Smith, and A. Naguib, "From theory to practice: An overview of MIMO space-time coded wireless systems," *IEEE Journal on Selected Areas in Communications*, vol. 21, no. 3, pp. 281-302,

2003.
[32] N. Wang, Y. Gao, and X. Zhang, "Adaptive spectrum sensing algorithm under different primary user utilizations," *IEEE Communications Letters*, vol. 17, no. 9, pp.1838-1841, 2013.
[33] S. Zhang and Z. Bao, "An adaptive spectrum sensing algorithm under noise uncertainty," in *2011 IEEE International Conference on Communications (ICC)*. Kyoto, Japan, 2011, pp. 1-5.
[34] G. Mahendru, A. K. Shukla, and L. M. Patnaik, "An optimal and adaptive double threshold-based approach to minimize error probability for spectrum sensing at low SNR tegime," *Journal of Ambient Intelligence and Humanized Computing*, vol. 13, pp. 3935-3944, 2022.
[35] Z. Bai, L. Wangand, and K. S. Kwak, "Different sensing durations-based cooperative spectrum sensing in cognitive radio systems," *Wireless Communications and Mobile Computing*, vol. 14, pp. 1522-1529, 2014.
[36] K. B. Letaief and W. Zhang, "Cooperative communications for cognitive radio networks," *Proceedings of the IEEE*, vol. 97, no. 5, pp. 878-893, 2009.
[37] E. Axell and E. G. Larsson, "Spectrum sensing of orthogonal space-time block coded signals with multiple receive antennas," in *2010 IEEE International Conference on Acoustics, Speech and Signal Processing*. Dallas, TX, USA, 2010, pp. 3110-3113.
[38] A. B. H. Hmida, S. Cherif, and H. Besbes, "Spectrum sensing based on STBC higher order statistics for cognitive radio systems," in *the Third International Conference on Communications and Networking*. Hammamet, Tunisia, 2012, pp. 1-5.
[39] H. H. Choi, K. Jang, and Y. Cheong, "Adaptive sensing threshold control based on transmission power in cognitive radio systems," in *2008 3rd International Conference on Cognitive Radio Oriented Wireless Networks and Communications (CrownCom 2008)*. Singapore, 2008, pp. 1-6.
[40] N. I. Miridakis, T. A. Tsiftsis, G. C. Alexandropoulos, and M. Debbah, "Simultaneous spectrum sensing and data reception for cognitive spatial multiplexing distributed systems," *IEEE Transactions on Wireless Communications*, vol. 16, no. 5, pp. 3313-3327, 2017.
[41] G. B. Giannakis, Z. Liu, X. Ma, and S. Zhou, *Space-Time Coding for Broadband Wireless Communications*. Hoboken, Nnew Jersey: John Wiley & Sons, 2007.
[42] E. G. Larsson and P. Stocia, *Space-Time Block Coding for Wireless Communications*. Cambridge, UK: Cambridge University Press, 2003.
[43] A. Nafkha and B. Aziz, "Closed-form approximation for the performance of finite sample-based energy detection using correlated receiving antennas," *IEEE Wireless Communications Letters*, vol. 3, no. 6, pp. 577-580, 2014.
[44] O. Tirkkonen, A. Boariu, and A. Hottinen, "Minimal non-orthogonality rate 1 space-time block code for 3+ Tx antennas," in *2000 IEEE Sixth International Symposium on Spread Spectrum Techniques and Applications*. Parsippany, NJ, USA, 2000, pp. 429-432.
[45] J. Wang and Q. T. Zhang, "A multitaper spectrum based detector for cognitive radio," in *2009 IEEE Wireless Communications and Networking Conference*. Budapest, Hungary, 2009, pp. 1-5.
[46] Q. T. Zhang, "Multitaper based spectrum sensing for cognitive radio: Design and performance," in *2011 IEEE 73rd Vehicular Technology Conference (VTC Spring)*. Budapest, Hungary, 2011, pp. 1-5.
[47] E. H. Gismalla and E. Alsusa, "New and accurate results on the performance of the multitaper-based detector," in *2012 IEEE International Conference on Communications (ICC)*. Ottawa, ON, Canada, 2012, pp. 1609-1613.